ACS APPLIED MATERIALS & INTERFACES

Research Article

www.acsami.org

Preparation Method of Crack-free PVDF Microfiltration Membrane with Enhanced Antifouling Characteristics

Sahng Hyuck Woo, Ju Sung Lee, Hyun Ho Lee, Jinwon Park, and Byoung Ryul Min*

Department of Chemical and Biomolecular Engineering, Yonsei University, 50 Yonsei-ro, Seodaemun-gu, 120-749, Seoul, South Korea

ABSTRACT: This study proposes a method to prepare a crack-free poly(vinylidene fluoride) (PVDF) microfiltration (MF) membrane with enhanced antifouling property. In the study, blending 4% poly(vinylidene fluoride)-*graft*-poly(sulfopropyl methacrylate) (PVDF-*g*-PSPMA) and 1.5% potassium perchlorate ($KClO_4$) led to crack prevention during membrane preparation via nonsolvent induced phase separation (NIPS) when compared with blending with 4% PVDF-*g*-PSPMA only (without $KClO_4$). The resulting crack-free membrane (A3) had both smooth surface structure and hydrophilicity in comparison with pristine PVDF membrane (A1). In addition, blending with PVDF-*g*-PSPMA and $KClO_4$ also allowed the A3 membrane to exhibit uniform pore size distribution (PSD) and smooth surface structure, compared with PVDF membrane commercially available from company "M" in Germany. The aforementioned properties led to antifouling characteristics in the crack-free membrane (A3). According to flux performances, flux recovery and cumulative permeate volume (between 120 and 240 min) of crack-free membrane (A3) were 11.41 and 17.41% superior to those of commercial membrane, respectively.

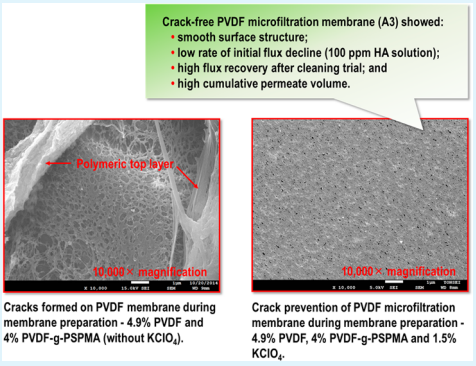

KEYWORDS: *crack prevention, potassium perchlorate ($KClO_4$), antifouling property, pore size distribution (PSD), flux recovery*

1. INTRODUCTION

Membrane separation and purification processing has been employed in a wide range of applications for food (e.g., dairy, beverage, fish) and batteries (e.g., vanadium redox flow battery, fuel cell).[1−5] In addition, water processing membranes are being used in the field of water treatment, including applications for drinking water, wastewater, brackish water, and seawater desalination; health protection purposes; high-quality water production; water supply expansion; low-cost water treatment; and water quality maintenance.[6−15] Attempts to improve membranes currently used in a variety of fields are being made through various studies on antifouling to address the issue of operational degradation from fouling and hydrophobic properties.[1−10] Membranes are prepared with organic material or inorganic material only, or a combination of the two. Among membrane materials, poly(vinylidene fluoride) (PVDF) has advantageous characteristics of high strength, thermal stability, and chemical resistance.[16−18] However, PVDF membranes are prone to fouling, which reduces permeate flux, decreases rejection, and increases energy consumption during filtration.[19−21] In particular, PVDF microfiltration (MF) membranes are usually vulnerable to humic acid (HA), which represents natural organic matter (NOM).[22] For that reason, research on antifouling membrane formation has been focused on the dilemma of HA fouling.[23−26] Among a broad range of methods, blending of graft copolymer has recently been reported as effective for antifouling characteristics enhancement.[23−26] In this method, functional polymeric material synthesized is blended in PVDF solution for antifouling membrane preparation. Other researchers have prepared PVDF membranes blended with poly(vinylidene fluoride)-*graft*-poly(hydroxyethyl methacrylate) (PVDF-*g*-PHEMA), poly(vinylidene fluoride)-graft−poly(oxyethylene methacrylate) (PVDF-*g*-POEM) and poly(vinylidene fluoride)-*graft*-poly(sulfobetaine methacrylate) (PVDF-*g*-PSBMA).[23−25]

However, it has not yet been clarified how the method of blending with synthesized graft copolymer causes the serious problem of crack formation of PVDF MF membranes through blending of PVDF solution with excessive hydrophilic graft copolymer during membrane preparation via nonsolvent induced phase separation (NIPS). Moreover, it has not yet been fully determined that blending with hydrophilic graft copolymer and $KClO_4$ is a solution which leads to crack prevention in PVDF MF membrane during membrane preparation, and the resulting crack-free membrane would exhibit antifouling characteristics during microfiltration of HA solution (100 ppm). If the formation of cracks in PVDF MF membrane can be prevented during membrane preparation despite blending with excessive hydrophilic graft copolymer, it will have useful application for the preparation of PVDF MF membranes with enhanced antifouling property.

The present study proposes a method to prepare crack-free PVDF MF membrane with enhanced antifouling characteristics. In the study, the authors discovered that a novel method of

Received: May 1, 2015
Accepted: July 14, 2015
Published: July 14, 2015

DOI: 10.1021/acsami.5b03797
ACS Appl. Mater. Interfaces 2015, 7, 16466−16477

Scheme 1. Synthesis Procedure of PVDF-g-PSPMA Copolymer

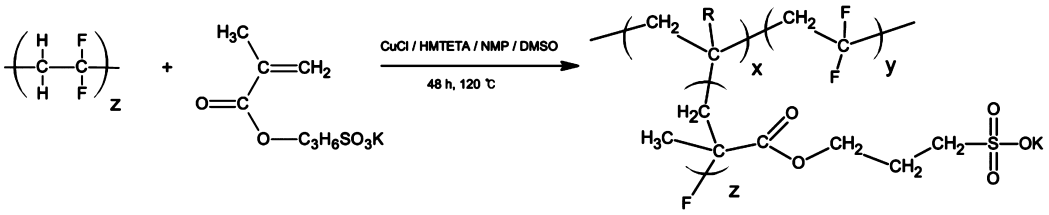

blending with 4% PVDF-*g*-PSPMA and 1.5% $KClO_4$ prevented PVDF MF membrane cracks, which are present when blending PVDF solution with 4% PVDF-*g*-PSPMA only (without $KClO_4$). The membrane (A3) prepared in this manner also had both smooth surface structure and increased hydrophilicity compared with the pristine PVDF membrane. In addition, the A3 membrane had uniform PSD and smooth surface superior to PVDF membrane commercially available from company "M" in Germany. Moreover, enhanced antifouling property was also demonstrated through various comparisons of flux decline rate (from 0 to 10 min), cumulative permeate volume, and flux recovery of the prepared and commercial membranes during microfiltration of 100 ppm of HA solution at 0.2 bar.

2. EXPERIMENTAL SECTION

2.1. Materials. Poly(vinylidene fluoride) (PVDF, Solef 6020, M_w: 700 000) was supplied by Solvay, Korea. 3-Sulfopropyl methacrylate potassium salt (SPMA, 98%), copper (I) chloride (CuCl, reagent grade, 97%), 1,1,4,7,10,10-hexamethyltriethylenetetramine (HMTETA), potassium perchlorate ($KClO_4$), and methanol were purchased from Sigma-Aldrich, Korea. *N*-Methyl-2-pyrrolidinone (NMP) was purchased from Kanto chemical. Dimethyl sulfoxide (DMSO, 99%) was purchased from Samchun Pure Chemical. Humic acid was purchased from Acros Organics, USA. Deionized (DI) water (18.2MΩ·cm) was supplied from ultrapure water plants (aqua MAX 370 series, Younglin, Korea).

2.2. Experimental Methods. *2.2.1. Synthesis of PVDF-g-PSPMA copolymer.* Prior to the preparation of the membranes via NIPS, polymerization method from a previous study was used for PVDF-*g*-PSPMA synthesis and precipitation.[27,28] PVDF powders (2 g) were dissolved in NMP (20 mL) in an Erlenmeyer flask for 4 h at 80 °C. In the vial, SPMA (12 g) was dissolved in DMSO (30 mL) for 4 h at 80 °C. After SPMA solution was added to the PVDF solution, CuCl (0.02 g) and initiator HMTETA (0.10 mL) were mixed into the solution. The Erlenmeyer flask was installed with an overhead stirrer, and the entrance of the Erlenmeyer flask was sealed with a rubber septum. The graft copolymer reaction mixture was bubbled with nitrogen gas using a purge needle and vent needle for 30 min while stirring at room temperature. The reaction vessel was then placed in a silicon oil bath that was preheated to 120 °C on a hot plate (PC-420D, Corning, Inc., Corning, NY), and the reaction was allowed to proceed for 48 h, as shown in Scheme 1. The resultant graft copolymer mixture was allowed to cool at room temperature, after which it was transferred into methanol for precipitation. The reaction product was purified by DMSO and precipitated into methanol a second time. Last, the graft copolymer was dried in an oven (Buil Science, Korea) under vacuum overnight at 60 °C, after which it was ground and kept in a sealed bottle. It is noted that (1) PSPMA homopolymer dissolves in methanol or water, (2) PVDF dissolves in NMP, but (3) PVDF graft copolymers only dissolve in DMSO and not in NMP.[28]

2.2.2. Preparation of PVDF Microfiltration Membranes. All of PVDF MF membranes were prepared via NIPS. To begin with, PVDF, the synthesized PVDF-*g*-PSPMA copolymer, and $KClO_4$ were blended within casting solutions in vials according to the composition described in Table 1 after synthesis of PVDF-*g*-PSPMA copolymer. Various casting solutions were blended with DMSO in a silicon oil bath on a hot plate at 80 °C. It should be noted that graft copolymers

Table 1. Chemical Compositions of PVDF Casting Solutions Blended with $KClO_4$, Alone or Together with PVDF-g-PSPMA

membranes	PVDF (wt %)	PVDF-*g*-PSPMA (wt %)	$KClO_4$ (wt %)	DMSO (wt %)
A1	5.7	0.0	0.0	94.3
A2	5.3	0.0	1.5	93.2
A3	4.9	4.0	1.5	89.6

are only soluble in DMSO and not in NMP. The casting solutions were cast with a gap distance of 150 μm by casting knife directly after they were poured on nonwoven fabric placed on a glass plate and then immersed into a coagulation bath filled with DI water for 5 min. The flat sheet membranes made in the coagulation bath were rinsed with DI water for 6 h, after which the membranes prepared in rinse bath were dehydrated in ambient conditions for 16 h. All the membranes were made to have average pore sizes of about 220 nm, similar to that of the commercially available PVDF membrane for accurate comparison of flux decline rate, permeate volume, and flux recovery. Average pore sizes (about 220 nm) of the A1, A2, and A3 membranes were controlled by PVDF content because blending of $KClO_4$ reduces average pore size of the membranes.[29]

2.3. Analytical Methods. *2.3.1. Graft Copolymer Characterizations. 2.3.1.1. FTIR-ATR.* Functional groups of the synthesized PVDF-*g*-PSPMA were verified using FTIR-ATR (Spectrum 100, PerkinElmer, Waltham, MA). The presence of ester and carbonyl groups (C−O single bonding and C═O double bonding) was analyzed through FTIR-ATR spectra of PVDF-*g*-PSPMA. The wavenumber range was set from 380 to 4000 cm^{-1}.

2.3.1.2. ^1H NMR. Grafting ratio of PSPMA in PVDF-*g*-PSPMA (on a mass basis) was confirmed through the spectra from 600 MHz ^1H NMR (AVANCE 600 MHz FT-NMR, Bruker, Germany) spectroscopy. Prior to conducting the grafting ratio confirmation, PVDF-*g*-PSPMA was blended with DMSO-d_6 (99.96 atom % D, Sigma-Aldrich, Korea), a solvent replaced with heavy hydrogen.[28]

2.3.1.3. Thermal Gravimetric Analysis (TGA). The thermal property of the synthesized PVDF-*g*-PSPMA was characterized via TGA data from STA (STA 8000, PerkinElmer, Waltham, MA). TGA test was performed under a nitrogen gas. The range of heating samples was from 30 to 800 °C at a rate of 14 °C/min. It was confirmed that PVDF was synthesized with SPMA as a weight loss percentage of PVDF-*g*-PSPMA copolymer during heating.

2.3.2. Membrane Characterizations. 2.3.2.1. Membrane Morphology, Crack Formation and Crack Prevention. A1, A2, A3, and commercial membranes were examined by FE-SEM (JSM-7001F/JSM-6701F, JEOL, Japan) at 10000× magnification. In addition, crack formation of 4.9% PVDF/4% PVDF-*g*-PSPMA blend membranes were confirmed during observation at 400, 500, 6000, and 10 000×. Fouling behavior on open membrane surface was observed at 5000× and 35 000× magnification. All membranes were coated with platinum (Pt) for 150 s prior to FE-SEM analysis.

2.3.2.2. Average Pore Size and Pore Size Distribution. Pore size distribution (PSD) analyses were accurately conducted with CFP (CFP-1200-AEL, Porous Materials, Inc., Ithaca, NY). All membranes were evaluated using the bubble point and N_2 gas flow setup as a function of the trans-membrane pressure increase, which is first estimated via the wet curve of the membrane with 1,1,2,3,3,3-hexafluoro-propene (Galwick solution as surface tension 15.9 dyn/

DOI: 10.1021/acsami.5b03797
ACS Appl. Mater. Interfaces 2015, 7, 16466−16477

cm^{-1}), and then via the dry curve of the membrane. Then, the average pore sizes and PSD were automatically calculated by PMI automated perm-porometer system software based on the following equation:[30,31]

$$D = \frac{4\gamma\cos\theta}{P} \quad (1)$$

where D and γ are the pore size and surface tension of the wetting liquid, respectively, θ is the contact angle of the wetting liquid, and P is the differential pressure.

2.3.2.3. Surface Roughness. AFM (XE-Bio, Park Systems, Korea) provided Surface roughness information on the A1, A2, A3, and commercial membranes for different compositions (Table 1). For AFM measurements, all the membranes were placed on slide glasses. Their surface roughness was observed by calculating the average roughness (R_a), the root average square of Z data (R_q), and the average difference between the five highest peaks and five lowest valleys (R_z) at a scan area of 5.0 × 5.0 μm. Noncontact AFM mode (NC-AFM) was applied at 0.4−0.5 Hz scanning rates.

2.3.2.4. Water Contact Angle. Hydrophilicity was characterized using water contact angle measurement (Phoenix 300, SEO). DI water was used as probe liquid. With DI water droplets of 20 μL put on the membrane surface, the average of water contact angles of each membrane were measured at three points after 3 s.

2.3.2.5. Flux Performances. Flux performance measurements were carried out for the observation of antifouling property of the membranes blended with PVDF-*g*-PSPMA and $KClO_4$. Permeate flux (L/m^2 hr), flux recovery (L/m^2 hr), normalized flux (J/J_0), and cumulative permeate volume (ml) were measured by a dead-end 44.5 mm diameter Amicon cell (Model 8050, Millipore) linked to an air-pressurized solution reservoir. Flux performance was obtained by measuring the hydraulic permeability (L_p) of high-concentration HA solutions (Molecular weight of HA: 1000−300 000 Da) of 100 ppm every 5 min (total 120 or 240 min by HA solution) at room temperature. Permeate flux was conducted after flux stabilization of 30 min by DI water. The pH of HA solution was adjusted to pH 7.012 ± 0.109 (R^2 = 96.5 ± 0.1) by addition of 0.1 M NaOH, using a pH meter (Orion DUAL STAR, Thermo Fisher Scientific, Waltham, MA). Transmembrane pressure was 0.2 bar, and the stirring speed was set to 400 rpm. Transmembrane flow rate was verified by timed collection with output (mass) examined using an electronic balance. Hydraulic permeability (L_p) was evaluated with the following equation:[32]

$$L_p = \frac{J}{\Delta P} \quad (2)$$

where ΔP is the applied pressure, and J is water filtrate flux.

2.3.2.6. Flux Recovery after Chemical Cleaning. To compare the results with the commercially available PVDF membrane, we regenerated membranes by chemical cleaning trial after permeate flux by soaking the fouled membranes in 0.1 M NaOH solution for 30 min. The cleaned membranes were flushed using DI water, after which the flux recovery was verified.[22]

3. RESULTS AND DISCUSSION

3.1. Graft Copolymer Characterization. Figure 1 shows the FTIR-ATR spectra of PVDF-*g*-PSPMA, indicating successful synthesis of PVDF and SPMA. The C═O double bonding of the ester group of PVDF-*g*-PSPMA copolymers was observed at 1716 cm^{-1}, while the sulfonic group as well as C−O ester group of synthesized PVDF-*g*-PSPMA copolymers were measured at 1160 cm^{-1}.[28] In order to identify polymerization, two peaks of PVDF-*g*-PSPMA copolymers and SPMA powders were compared at 1637 cm^{-1}. In comparison with the spectrum of the SPMA powders at 1637 cm^{-1}, the intensity of PVDF-*g*-PSPMA copolymer peaks decreased due to the change from an alkene group (C═C double bonding) to an alkane group (C−C single bonding) through polymerization. In addition, the spectral peak of PVDF-*g*-PSPMA copolymers was more clearly

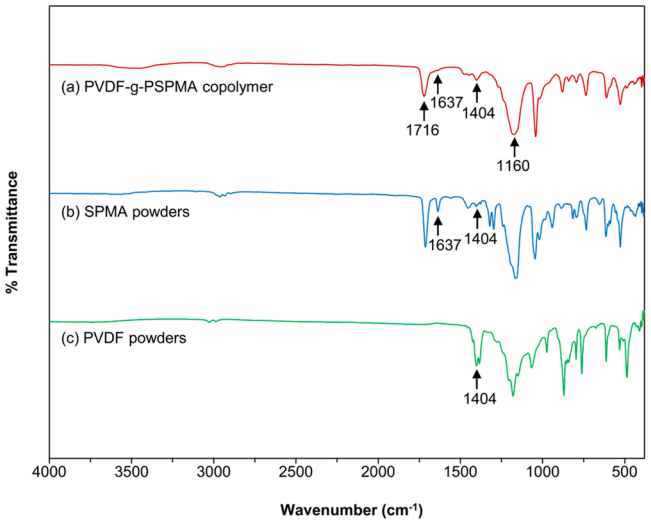

Figure 1. FTIR-ATR spectra of (a) PVDF-*g*-PSPMA copolymer, (b) SPMA powder, and (c) PVDF powder.

observed than the SPMA peak at 1404 cm^{-1}, which is due to increase in alkane CH_2 of PVDF-*g*-PSPMA synthesized with PVDF and SPMA.

The ^{1}H NMR spectra of the synthesized PVDF-*g*-PSPMA were also observed to confirm successful polymerization. Figure 2 shows the ^{1}H NMR spectra generated to confirm the grafting

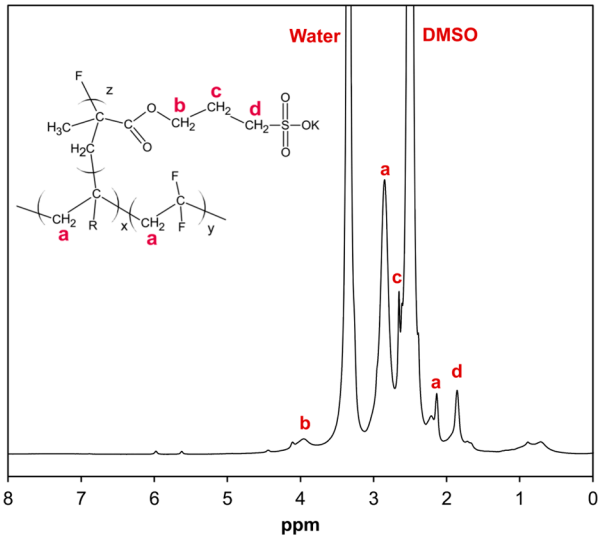

Figure 2. ^{1}H NMR spectra of PVDF-*g*-PSPMA copolymer. ^{1}H NMR (600 MHz, [D_6] DMSO): (a) δ = 2.1 (t, J = 3.0 Hz, 2H, head to tail), 2.8 (quint, J = 3.0 Hz, 2H, head to head), (b) 4.0 (2H, −O−CH_2−), (c) 2.7 (2H, −CH_2−CH_2−CH_2−), and (d) 1.9 (2H, −CH_2−SO_3K−) ppm.

of PSPMA onto the PVDF-*g*-PSPMA. The peaks at 2.5 and 3.3 ppm represent DMSO and water, while the peaks of head to tail (ht) and head to head (hh) bonding arrangements of PVDF appear at 2.8 and 2.1 ppm, respectively. The peaks of the PSPMA grafted onto the PVDF, presumably due to the alkyl CH_2 bonded with the sulfopropyl methacrylate, appear at 4.0, 2.7, and 1.9 ppm. Grafting ratio on a mass basis is determined by the integral ratio of signal a, originating from the hh (2.8 ppm) and ht (2.1 ppm) of PVDF, and signal b, originating from

DOI: 10.1021/acsami.5b03797
ACS Appl. Mater. Interfaces 2015, 7, 16466−16477

the hydrogen atom (4.0, 2.7, or 1.9 ppm) existent in PSPMA, calculated according to the following equations:[28]

$$f_{\mathrm{PVDF}} = \frac{(I_a \times 64/2)}{(I_a \times 64/2 + I_b \times 248/2)} \quad (3)$$

$$f_{\mathrm{PSPMA}} = \frac{(I_b \times 248/2)}{(I_a \times 64/2 + I_b \times 248/2)} \quad (4)$$

where I_a (2.8 and 2.1 ppm) and I_b (4.0 ppm) are the integrations of the signals originating from the PVDF and PSPMA, respectively, and 64 and 248 represent the molar masses of the repeat units of PVDF and PSPMA, respectively. According to the above equations, the ratio of PSPMA grafted in PVDF-*g*-PSPMA was calculated at 27% on a mass basis.

Figure 3 provides TGA data of PVDF powder and PVDF-*g*-PSPMA graft copolymer. PVDF started declining at about

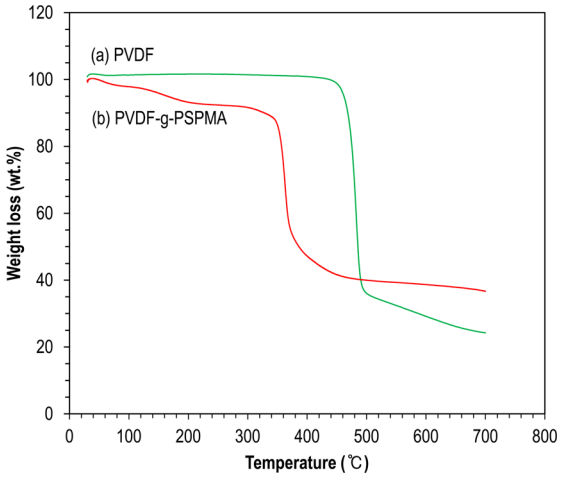

Figure 3. TGA data on (a) PVDF powder and (b) PVDF-*g*-PSPMA copolymer.

446.4 °C, which shows decomposition to approximately 30 wt %. However, PVDF-*g*-PSPMA copolymer indicated decomposition to about 20 wt % at approximately 350.6 °C. This may be attributed to the decomposition of the sulfonic acid groups.[28] Moreover, the weight loss of PVDF-*g*-PSPMA copolymer was observed around 100 °C, mostly attributable to the loss of adsorbed water by hydroscopic characteristics. According to characterization, it was determined that PVDF was successfully synthesized with SPMA.

3.2. Membrane Characterizations. CFP is usually used as much as FE-SEM in order to determine pore sizes of membranes.[30,31,33] In this study, average pore size and PSD were measured using CFP data. This is because (1) accurate pore sizes could not be measured using FE-SEM due to networks of several layers of membrane samples, and (2) there is difficulty in using FE-SEM to estimate pore sizes owing to thickness of coating layer. FE-SEM images show smaller pore sizes than actual pore sizes of membrane samples.[34,35] The working principle of CFP is based on the bubble point and gas permeate on tests.[30,31,33] As noted, the average pore sizes (about 220 nm) of A1, A2, and A3 membranes were controlled by PVDF content as shown in Table 1, as blending of $KClO_4$ reduces average pore size of the membranes.[29] Attempts to make the average pore sizes of all the prepared membranes about 220 nm, similar to that of the commercially available PVDF membrane fabricated at about 220 nm by the manufacturing company, were successful. This is because comparisons of permeate flux, flux recovery, and permeate volume of membranes can be more accurately conducted when average pore sizes of membranes tested are similar (about 220 nm). Average pore sizes of all membranes are automatically computed by PMI automated perm-porometer system software based on average flow pressure, which corresponds to the intersection of the wet curve with the half-dry curve measured by CFP.[30,31] Average pore sizes of membranes were similar: 229.4, 225.5, 223.2, and 240.4 nm for A1, A2, A3 and commercial membranes, respectively. Meanwhile, Figure 4 represents the cumulative PSD (%) curves for all membranes. Although approximately 40% of pores were observed around 160 nm, the average pore size of the commercial membrane was about 220 nm. The reason for this variance is that the commercial membrane, which was fabricated at average pore size of about 220 nm by the manufacturing company, has randomly distributed pore sizes on the surface. That is, large pore sizes varied between 240.9 and 445.9 nm, allowed commercial membrane to have average pore size of about 220 nm. However, large pore sizes between 230.8 and 590.6 nm for A1, A2, and A3 membranes showed around 0.1%. The pore sizes of the A1, A2, and A3 membranes measured by CFP was mostly distributed at about 220 nm, and also had average pore sizes of between 220 and 230 nm. PVDF membranes, blended with $KClO_4$ alone (by a maximum of about 97% at 225.4 nm) or together with PVDF-*g*-PSPMA (by a maximum of about 91% at 223.3 nm), improved uniformity of pore size, compared with pristine PVDF membrane with no additives (by a maximum of about 85% at 229.3 nm).

A1, A2, and A3 membranes with about 220 nm average pore size were prepared, controlled by PVDF content because blending of $KClO_4$ reduces average pore size. However, membrane blended with 4% PVDF-*g*-PSPMA only (without $KClO_4$) caused serious problems, as shown in Figure 5, forming cracks and polymeric fragments on the membrane during membrane preparation via NIPS. Hence, the average pore size of the membrane blended with 4% PVDF-*g*-PSPMA only (without $KClO_4$) could not be controlled at about 220 nm, unlike those of the A1, A2, A3, and commercial membranes. Blending of 1, 2, or 3% PVDF-*g*-PSPMA only (without $KClO_4$) also caused formation of membrane cracks. Figure 5 shows the various negative effects. Figure 5b shows the part under the top layer exposed along with the top layer due to the broken top layer, with clearly different appearance to either side of the dotted red line. In particular, in Figure 5, panels c and e show the formation of cracks, which include polymeric fractions, and the part without cracks displays randomly scattered fractions, as shown in panels d and f. Also, some parts of nonwoven fabric were exposed in dotted red boxes, as shown in Figure 5e. These results may be attributed to the blending of excessive hydrophilic graft copolymer (i.e., PVDF-*g*-PSPMA), which may cause crack formation during membrane preparation via NIPS. The formation of cracks on the membrane surface was, however, prevented by blending with 4% PVDF-*g*-PSPMA and 1.5% $KClO_4$ (A3 membrane), and the crack formation problem was largely solved, as shown in Figure 6c. This means that blending with 4% PVDF-*g*-PSPMA and 1.5% $KClO_4$ can prevent cracks and control average pore size (i.e., about 220 nm), compared with blending with PVDF-*g*-PSPMA only (without $KClO_4$).

Figure 6a–d shows the FE-SEM images of A1, A2, A3, and commercial membranes estimated at 10 000×. The A1, A2, and

DOI: 10.1021/acsami.5b03797
ACS Appl. Mater. Interfaces 2015, 7, 16466–16477

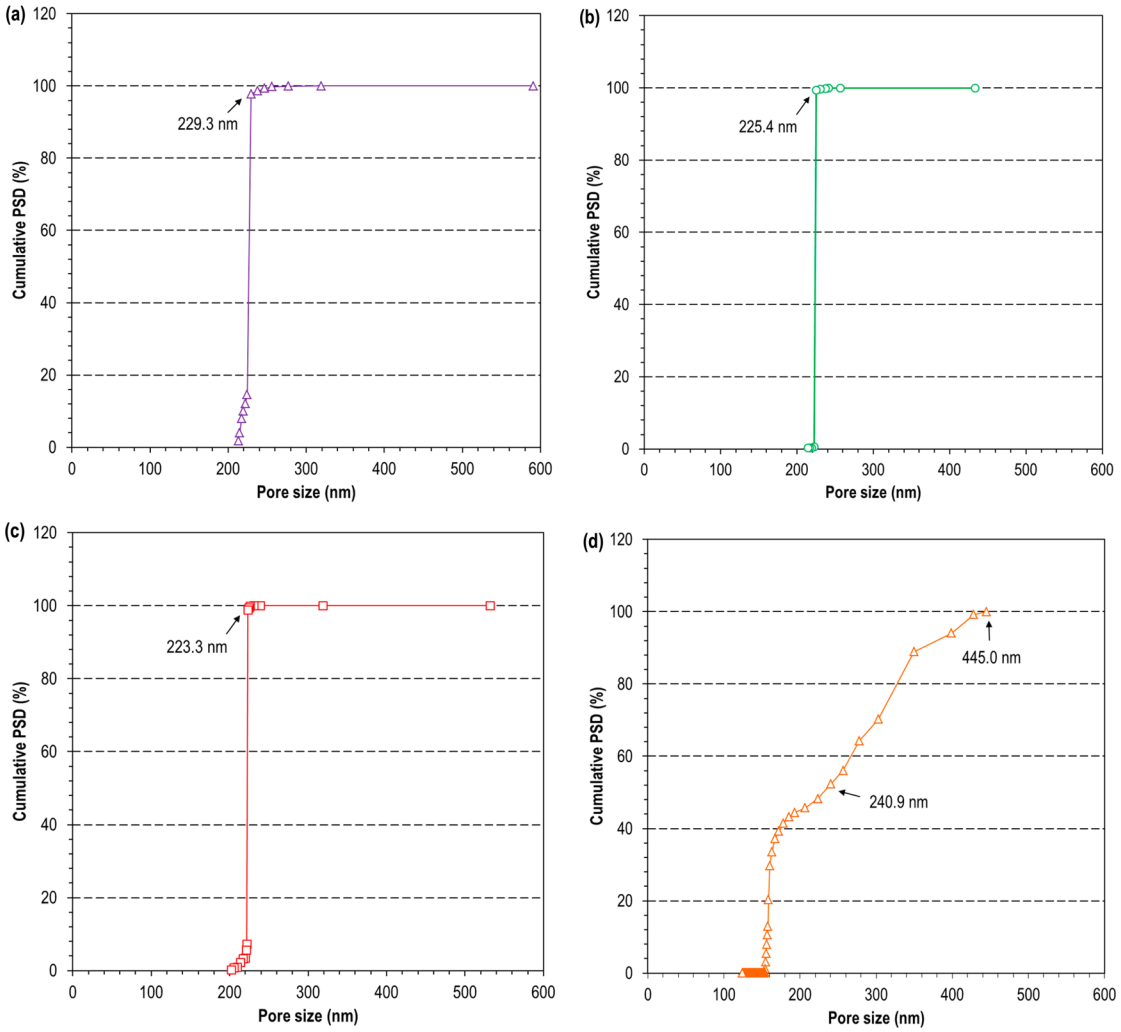

Figure 4. Cumulative pore size distribution (PSD) images measured by CFP of (a) A1 (pristine PVDF), (b) A2 (PVDF/$KClO_4$), (c) A3 (PVDF/PVDF-*g*-PSPMA/$KClO_4$), and (d) commercial membranes.

A3 membranes tested, as shown in Figure 6a–c, indicated distributed pore sizes similar to those displayed by data measured by CFP (Figure 4a–c). However, the reason that pore sizes observed by FE-SEM show smaller pore sizes than actual pore sizes measured by CFP may be thickness of coating layer of membrane samples.[34,35] In addition, it was confirmed that membrane crack formation was prevented by blending with PVDF-*g*-PSPMA and $KClO_4$, as shown in Figure 6c. More specifically, exposure of the part under the top layer as well as formation of cracks, caused by blending of PVDF-*g*-PSPMA only (without $KClO_4$), could be prevented. Figure 5e shows membrane with numerous cracks at 10000× magnification, whereas Figure 6c shows crack-free membrane (A3) at the same magnification. Such crack prevention may be attributed to the interaction between $KClO_4$ and phase inversion kinetics. This means that 1.5% $KClO_4$ in the A3 casting solution resulted in stronger interaction between $KClO_4$ and solvent (i.e., DMSO), compared with that between $KClO_4$ and polymer (i.e., PVDF and PVDF-*g*-PSPMA). Strong interaction between $KClO_4$ and solvent (i.e., DMSO) can also be inferred from the increase in viscosity of the A3 casting solution. The increase in viscosity caused by interaction between salt and solvent was studied in numerous papers.[29,36,37] As for viscosity values of casting solutions measured using viscometer (LVDV-II+, Brookfield, Middleboro, MA) at 80 °C, the viscosity of casting solution for 4.9% PVDF/4% PVDF-*g*-PSPMA blend membrane was 210.0 cP due to the absence of $KClO_4$, whereas that for 4.9% PVDF/4% PVDF-*g*-PSPMA/1.5% $KClO_4$ membrane (A3) was 319.9 cP. As a result, the aforementioned $KClO_4$/DMSO interaction and viscosity increase in the A3 casting solution led to reduced DMSO activity and increased thermodynamic stability. Accordingly, the driving force for DMSO outflow of the polymeric film declined, thereby resulting in the formation of crack-free membrane (A3). Meanwhile, as shown in Figure 6d, pores sizes larger or smaller than 220 nm were frequently and repeatedly observed on the surface of the commercial membrane with approximately 220 nm average pore size at 10000×, in contrast to the A1, A2, and A3 membranes measured at the same magnification. According to PSD data measured by CFP (Figure 4), the randomly distributed pore sizes of the commercial membrane surface is presumably attributable to networks of several layers, in comparison with relatively narrow range of PSD of the A1, A2, and A3 membranes. In addition, the FE-SEM surface image of the commercial membrane revealed a more uneven surface than the A1, A2, and A3 membranes.

As shown in Figure 7 and Table 2, A1 membrane (pristine PVDF membrane) showed 166.433 nm as root average square

DOI: 10.1021/acsami.5b03797
ACS Appl. Mater. Interfaces 2015, 7, 16466–16477

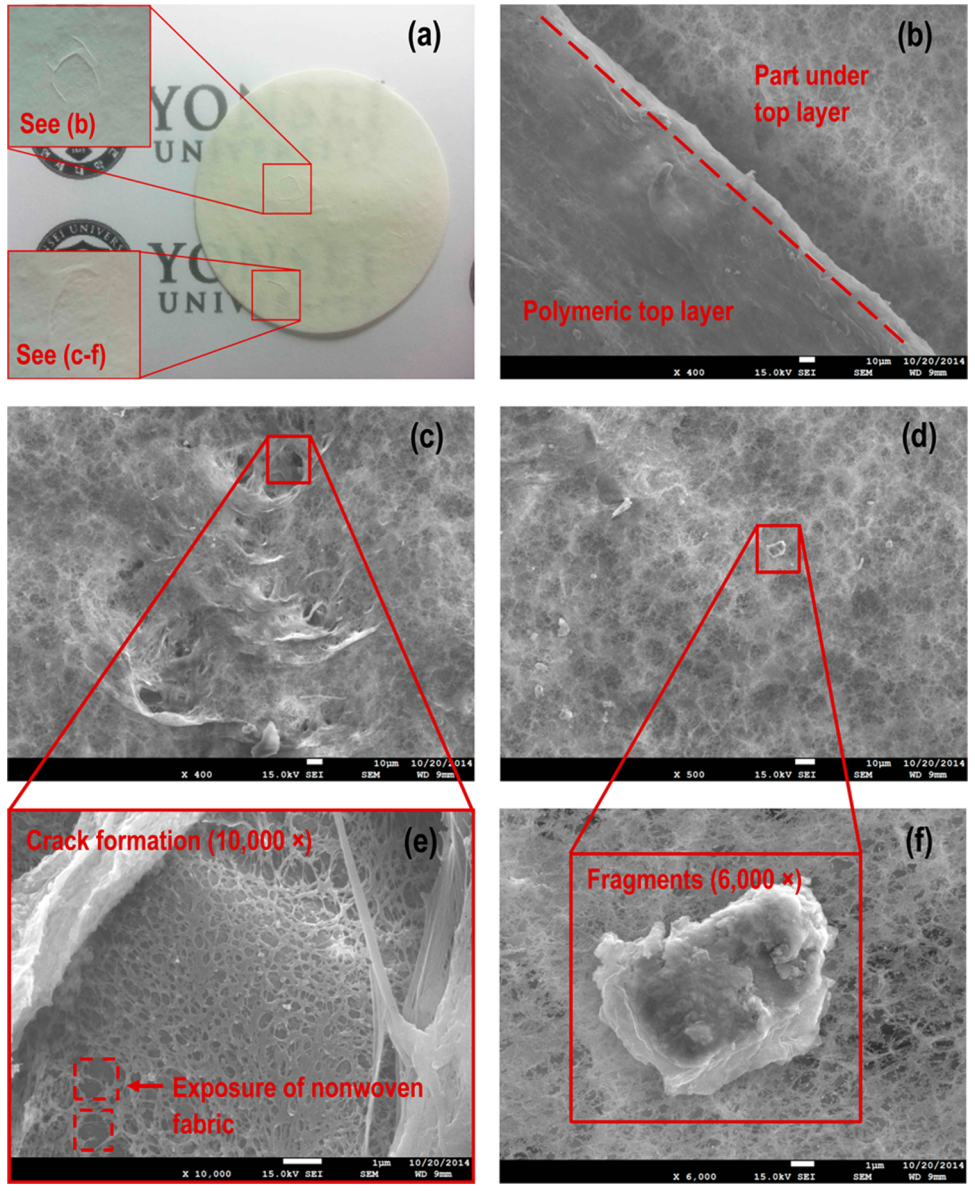

Figure 5. (a) Photo and (b–f) FE-SEM images regarding crack formation and fragments of 4.9% PVDF/4% PVDF-*g*-PSPMA blend membrane (without blending with 1.5% $KClO_4$).

(RMS) roughness (R_q). However, blending of $KClO_4$ only or together with PVDF-*g*-PSPMA formed the membrane with smooth surface structure. That is, A2 membrane (PVDF membrane blended with $KClO_4$ only) formed a smoother surface than commercial and pristine PVDF membranes. Among all membranes tested, A3 membrane showed the smoothest surface, with 44.608 nm as R_q roughness. This result may be attributed to the interaction between $KClO_4$ and DMSO. Blending of $KClO_4$ only or together with PVDF-*g*-PSPMA led to decreased DMSO activity and increased thermodynamic stability of casting solutions, resulting in formation of the smooth membrane surface during phase inversion process.[29] In contrast, the surface roughness of the commercial membrane was the greatest, with 838.308 nm R_q roughness, or about 18.8 times that of the A3 membrane.

PVDF has an essentially hydrophobic characteristic. The contact angle of A1 membrane (pristine PVDF membrane) was evaluated by water contact angle measurement, with a contact angle value of 73.46° as noted in Table 2. The A2 membrane showed contact angle values similar to A1 membrane as $KClO_4$ was mostly dissolved when the membranes were immersed into coagulation bath filled with DI water during membrane preparation. The A3 membrane showed a lower contact angle value (i.e., 56.21°) than those of A1 and A2 membranes. This result is attributable to the hydrophilic characteristics and smooth surface formation caused by sulfonic group of PVDF-*g*-PSPMA and $KClO_4$. In other words, the problem of crack formation of membrane caused by blending of only 4% PVDF-*g*-PSPMA (without $KClO_4$) was solved by a novel method to blend with 1.5% $KClO_4$ and 4% PVDF-*g*-PSPMA, and this method, in turn, led to increased hydrophilicity of the A3 membrane compared with the A1 or A2 membranes. (Blending of 1, 2, or 3% PVDF-*g*-PSPMA only also causes formation of membrane cracks without blending with $KClO_4$). On the other hand, the commercial membrane was the most hydrophilic among all membranes tested.

To observe flux decline rate, flux recovery, and cumulative permeate volume of the prepared and commercial membranes,

DOI: 10.1021/acsami.5b03797
ACS Appl. Mater. Interfaces 2015, 7, 16466–16477

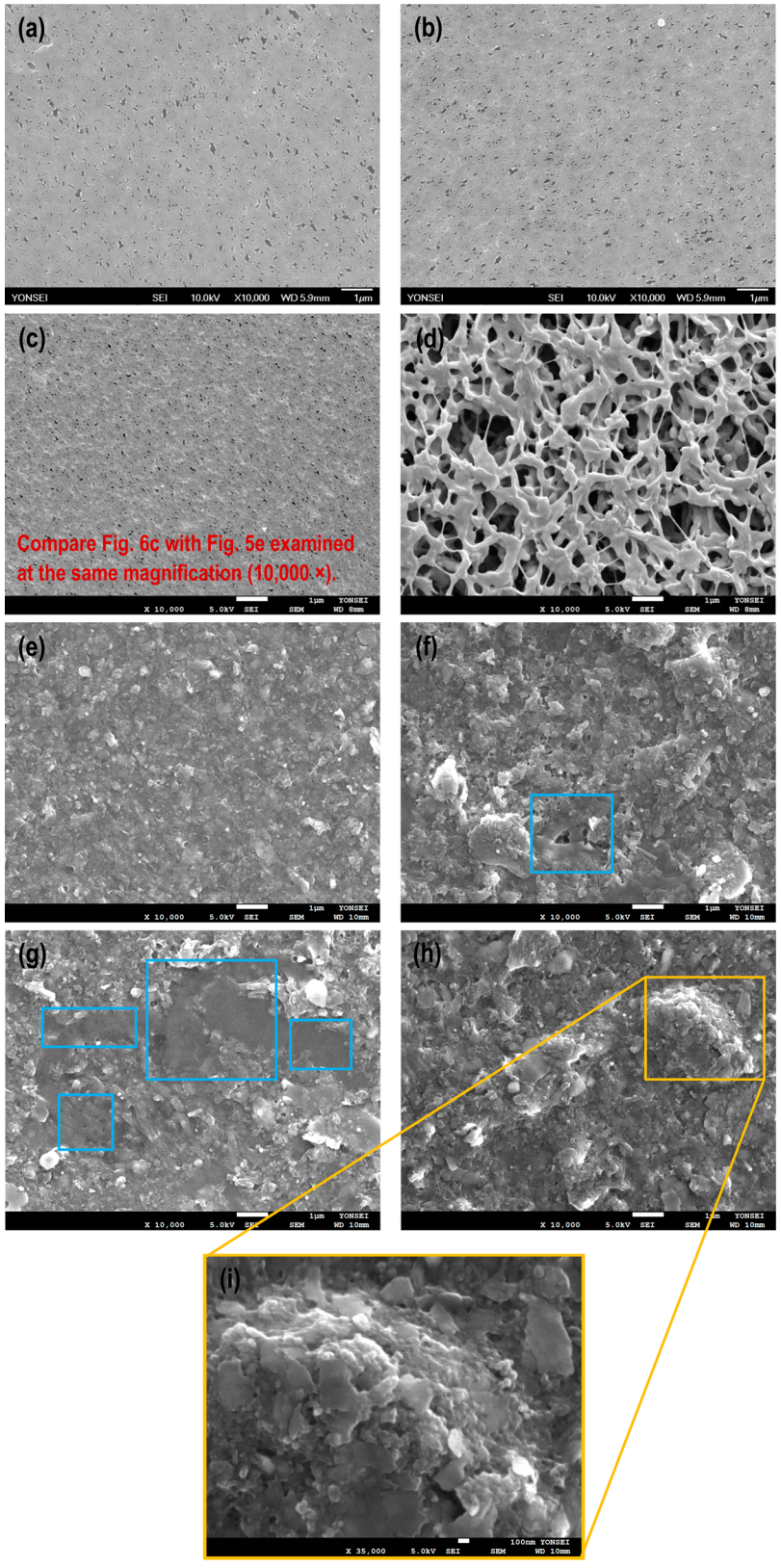

Figure 6. FE-SEM images of (a) clean A1 (pristine PVDF), (b) clean A2 (PVDF/$KClO_4$), (c) clean A3 (PVDF/PVDF-*g*-PSPMA/$KClO_4$), (d) clean commercial membranes, (e) fouled A1 (pristine PVDF), (f) fouled A2 (PVDF/$KClO_4$), (g) fouled A3 (PVDF/PVDF-*g*-PSPMA/$KClO_4$), (h) fouled commercial, and (i) fouled commercial membranes (35 000×) after 15 min.

we conducted flux tests during microfiltration of 100 ppm of HA solution at 0.2 bar. Figure 8 indicates the permeate flux of A1, A2, A3, and commercial membranes. Both A1 and A2 membranes, with relatively higher contact angle values, had lower permeate flux than the A3 and commercial membrane throughout the test. The A1 membrane showed higher

DOI: 10.1021/acsami.5b03797
ACS Appl. Mater. Interfaces 2015, 7, 16466−16477

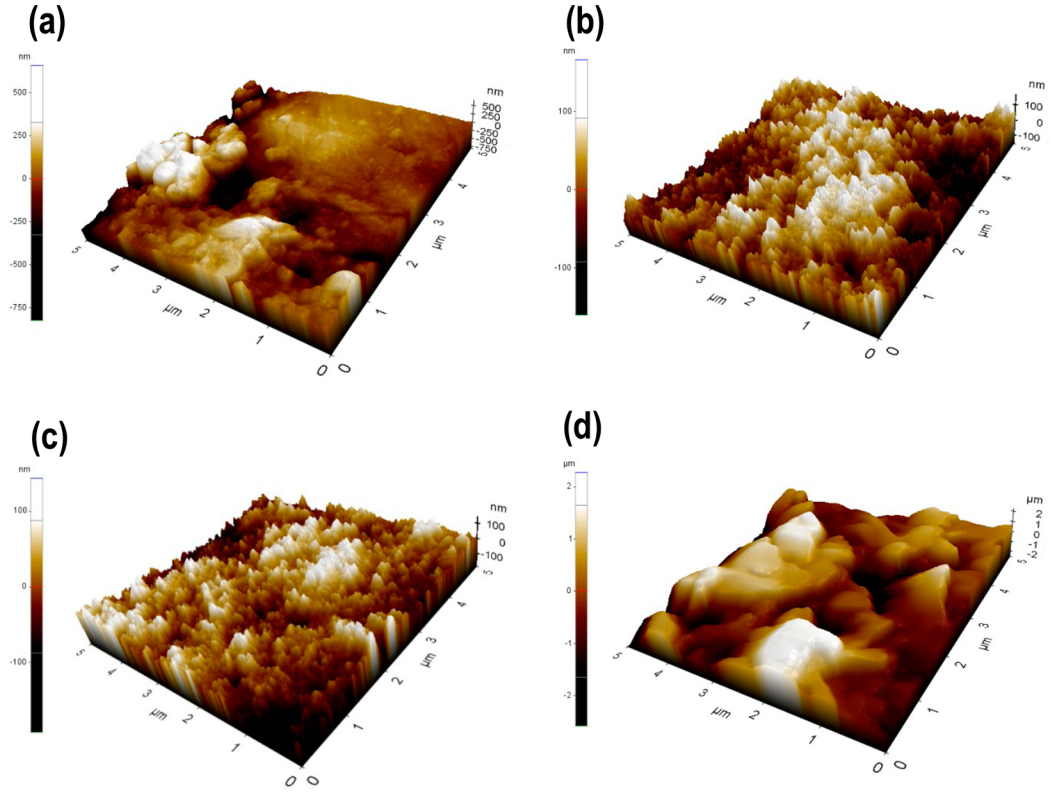

Figure 7. Surface roughness images measured by AFM of (a) A1 (pristine PVDF), (b) A2 (PVDF/$KClO_4$), (c) A3 (PVDF/PVDF-*g*-PSPMA/$KClO_4$), and (d) commercial membranes.

Table 2. Water Contact Angle and Surface Roughness Values of the A1, A2, A3 and Commercial Membranes

membranes	contact angle (deg)	surface roughness		
		R_q (nm)	R_a (nm)	R_z (nm)
A1 (No additives)	73.46	166.433	121.706	1441.586
A2 (1.5% $KClO_4$)	72.89	47.013	37.931	321.014
A3 (4% PVDF-*g*-PSPMA/1.5% $KClO_4$)	56.21	44.608	35.086	324.350
commercial membrane	36.34	838.308	681.110	4798.726

permeate flux than the A2 membrane before 10 min due to the difference between their average pore sizes. However, permeate flux of the A2 membrane was superior to that of the A1 membrane from 10 to 120 min even though the A2 membrane had smaller average pore size than A1 membrane. The results, as shown in Figure 7a,b and Table 2, are presumably attributable to smoother surface than A1 membrane,[34] and hence, it was confirmed that the blending of only 1.5% $KClO_4$ had a favorable effect on permeate flux during filtration of 100 ppm of HA solution at 0.2 bar. Meanwhile, commercial membrane displays high initial flux due to its hydrophilic property. However, commercial membrane shows that a rapid decline in flux (from 591.20 L/m^2 hr to 358.26 L/m^2 hr) compared with A3 membranes for the first 10 min. Figure 6e–i displays FE-SEM images of membrane surfaces fouled by HA solution after 15 min. It was confirmed that cake layer formation occurred on membrane surfaces. According to Figure 6e,f, the extent of fouling of the A2 membrane (see blue box) was not as great as that of the A1 membrane with rough surface. In particular, fouling of the commercial membrane, despite greater hydrophilicity, was severe compared with the A3

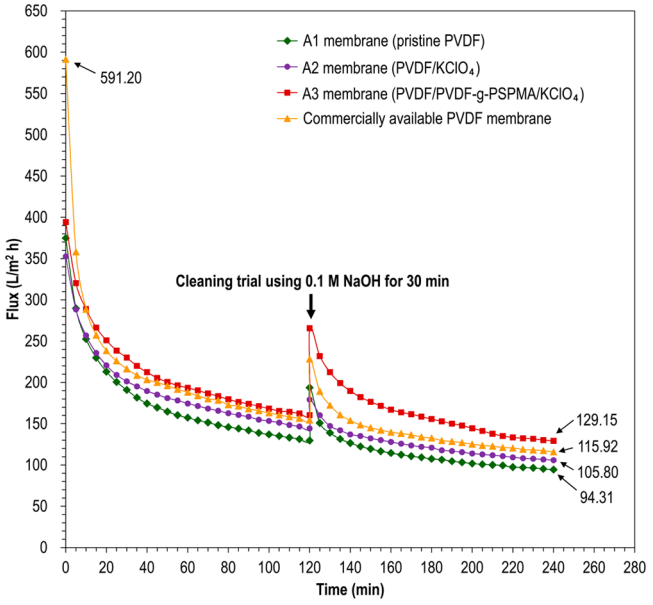

Figure 8. Permeate flux and after-cleaning flux recovery (L/m^2 h) of A1 (pristine PVDF), A2 (PVDF/$KClO_4$), A3 (PVDF/PVDF-*g*-PSPMA/$KClO_4$), and commercial membranes during microfiltration of 100 ppm of HA solution at 0.2 bar.

membrane. As shown within the blue box in Figure 6g, fouling of the A3 membrane surface was less than that of the commercial membrane. However, there were hills of about 2–3 μm diameter on the commercial membrane surface as shown in yellow box in Figure 6h,i. This result may be attributable to fouling problem at a higher HA solution filtration rate. The

DOI: 10.1021/acsami.5b03797
ACS Appl. Mater. Interfaces 2015, 7, 16466–16477

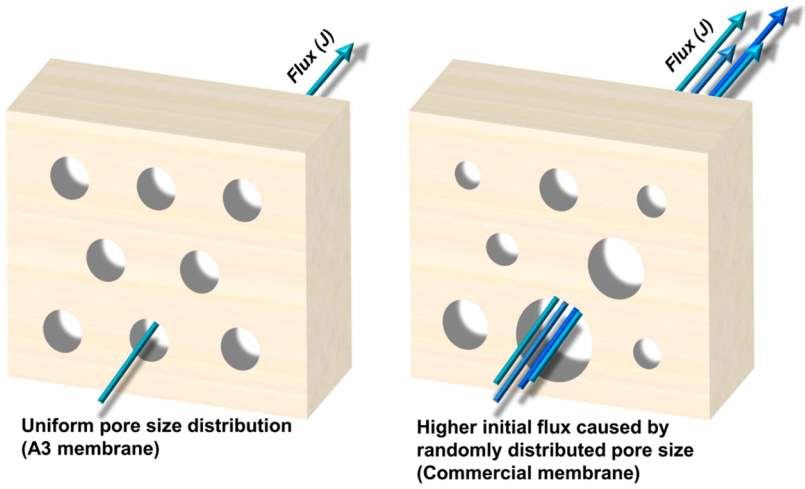

Figure 9. Uniform pore size distribution of (left) A3 (PVDF/PVDF-*g*-PSPMA/$KClO_4$) membrane and (right) randomly distributed pore sizes of commercial membrane.

phenomenon may be explained through the Hagen−Poiseuille equation:[39]

$$J \propto d_p^4 \tag{5}$$

where d_p^4 is the pore size, and J is the water filtrate flux. Flux (J) is proportionate to 4 times the pore size (d_p^4), and so, the commercial membrane, with the larger pore size than the A3 membrane, displays higher permeate flux for the first 10 min, as the average pore size of the commercial membrane was 240.4 nm, compared with 223.2 nm for the A3 membrane.[38,39] In other words, because the flux (J) of the larger pores (d_p^4) is higher than that of the smaller pores (d_p^4), the commercial membrane displays higher permeate flux than the A3 membrane for the first 10 min.

In conclusion, as shown in Figure 4c,d, the random distribution of the pore size on the commercial membrane surface means that it has relatively larger pores than the A3 membrane, which results in higher permeability (Figure 9). Accordingly, a greater amount of the 100 ppm of HA feed solution (i.e., HA macromolecules) is rapidly adsorbed to the commercial membrane, causing the accelerated decline of permeate flux for the first 10 min.[39] In contrast, A3 membrane exhibited a slower rate of decline in flux than the commercial membrane for the first 10 min but higher permeate flux after 15 min based on its uniform PSD, confirming superior antifouling characteristics. In addition to the average pore size and randomly distributed pore size, surface roughness is also a cause of rapid permeate flux decrease. The commercial membrane, which had a greater surface roughness than the A3 membrane by approximately 794 nm (Table 2), indicated rapid permeate flux and high permeability for the first 10 min, which in turn worsened its fouling. In addition, HA accumulates in greater amounts and more readily in the rough valleys of the commercial membrane due to its surface roughness, which presumably accelerates deposition on the membrane surface, thereby causing a dramatic decline of permeate flux.[34] Meanwhile, the A3 membrane displayed better antifouling characteristics than the commercial membrane, presumably because blending with $KClO_4$ and PVDF-*g*-PSPMA causes uniform PSD as well as smooth surface structure, which do not readily allow HA fouling. Due to these characteristics, the A3 membrane, with its relatively uniform PSD and smooth surface, showed higher permeate flux than the commercial membrane after 15 min, and superior antifouling property to the 3.84% (5.93 L/m^2 hr difference at 0.2 bar) of the commercial membrane at 120 min.

After conducting permeate flux tests for 120 min (from 0 to 120 min), the fouled A1, A2, A3, and commercial membranes were soaked in 0.1 M NaOH for 30 min and rinsed with DI water to remove remnant NaOH. As shown in Figure 8, flux recovery of the commercial membrane was 22.91 and 9.57% superior to those of the A1 and A2 membrane after 240 min, respectively, which may be due to the greater hydrophilicity of the commercial membrane than that of the A1 and A2 membranes. However, the regeneration rate of the A3 membrane was superior to that of the commercial membrane after cleaning trials. The A3 membrane exhibited a flux recovery superior to the commercial membrane after cleaning. Its flux recovery was 11.41% (13.23 L/m^2 h difference at 0.2 bar) higher than that of the commercial membrane after 240 min. Moreover, as can be seen in Figure 10, permeate volume of A3 membrane was superior to those of A1, A2 and commercial membranes after cleaning trial. In particular, the gap of the A3 and commercial membranes in the cumulative permeate volume was 17.41% (66.82 mL difference at 0.2 bar) between 120 and 240 min even though there was almost no difference between the two from 0 to 120 min. In addition, while the cumulative permeate volume of the 100 ppm of HA solution which passed through A3 membrane during the 120 min (from 120 to 240 min) was 17.41% greater than that of the commercial membrane, permeate flux of the cleaned commercial membrane is still lower than that of the A3 membrane, which means that much more fouling occurs from 120 to 240 min. These results indicate that flux recovery of A3 membrane was superior to that of commercial membrane.

Until now, flux performances were analyzed for four membranes with similar average pore sizes (i.e., about 220 nm). Nevertheless, the comparison of fouling behavior of four different membranes may be still not appropriate. This may be due to different initial flux (J) of membranes during the filtration of HA solution between 0 and 10 min (Figure 8), despite the similar average pore sizes. For this reason, HA solution filtrate flux (J) was normalized by J_0, which is the clean water flux evaluated just before HA solution filtration, according to the normalized flux (J/J_0) experiment studied by

DOI: 10.1021/acsami.5b03797
ACS Appl. Mater. Interfaces 2015, 7, 16466−16477

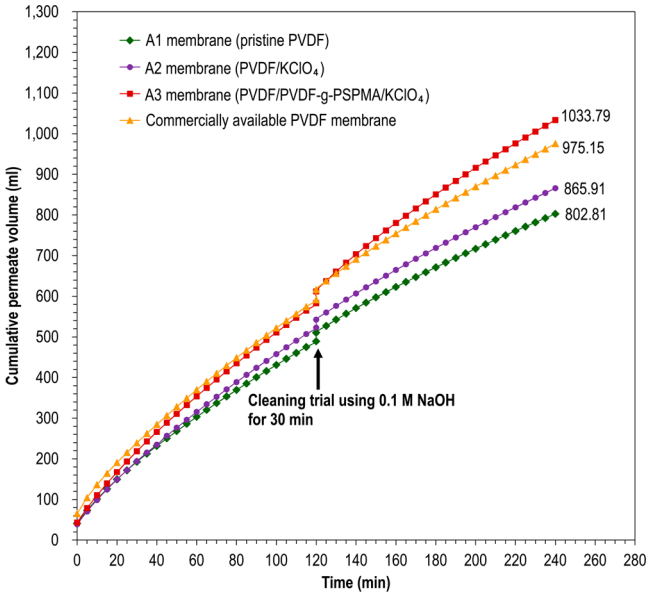

Figure 10. Cumulative permeate volume (ml) of A1 (pristine PVDF), A2 (PVDF/$KClO_4$), A3 (PVDF/PVDF-*g*-PSPMA/$KClO_4$), and commercial membranes during microfiltration of 100 ppm of HA solution at 0.2 bar.

Zydney's group.[22] The J_0 values for membranes were similar: 784.56 L/m^2 h (2.18 × 10^{-4} m/s), 713.60 L/m^2 h (1.98 × 10^{-4} m/s), 683.47 L/m^2 h (1.90 × 10^{-4} m/s), and 745.16 L/m^2 h (2.07 × 10^{-4} m/s) for A1, A2, A3 and commercial membranes at 0.2 bar, respectively. This means that the J values for membranes were varied, whereas the J_0 values for them were similar to only small differences. As shown in Figure 11, all the J/J_0 values indicated below 0.80 because the J_0 values for all membranes were high compared with their J values. Rapid flux decline (from 0.79 to 0.38) for commercial membrane was the greatest among membranes tested for initial 10 min, and it was

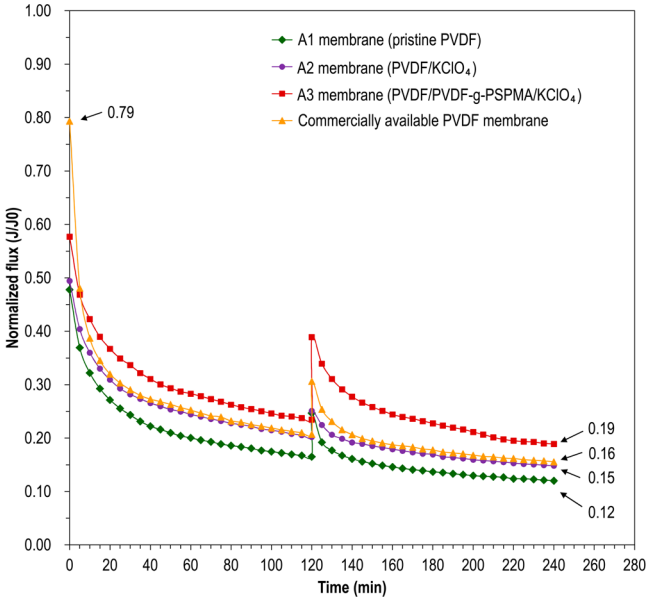

Figure 11. Normalized flux (J/J_0) of A1 (J_0 = 784.56 L/m^2 h), A2 (J_0 = 713.60 L/m^2 h), A3 (J_0 = 683.47 L/m^2 h), and A4 (J_0 = 745.16 L/m^2 h) membranes during microfiltration of 100 ppm of HA solution at 0.2 bar.

confirmed that A3 membrane ultimately exhibited final normalized flux 0.03 superior to that of commercial membrane. Additionally, it was demonstrated that chemical cleaning allowed A3 membrane to show flux recovery superior to those of A1, A2, and commercial membranes. However, A1 and A2 membranes displayed low normalized flux in comparison with A3 and commercial membranes after 240 min. Based on characterizations, these results may be because blending with PVDF-*g*-PSPMA and $KClO_4$ prevented crack formation in the membrane during membrane preparation, and the resulting crack-free membrane (A3) had both increased hydrophilicity and smoother surface structure compared with those of the pristine PVDF membrane. Moreover, membrane (A3) showed smoother surface structure as well as uniform PSD in comparison to the commercial membrane. Without confirmation of crack prevention by blending of PVDF-*g*-PSPMA and $KClO_4$, membrane with such characteristics could not be prepared. The aforementioned properties led to the crack-free membrane (A3) to have antifouling property, including flux decline rate, permeate volume, and flux recovery after chemical cleaning superior to those of the commercial membrane despite greater hydrophobic property.

4. CONCLUSION

Cracks formed during membrane preparation via NIPS can be prevented by blending with 4% PVDF-*g*-PSPMA and 1.5% $KClO_4$, compared with blending with 4% PVDF-*g*-PSPMA alone (without $KClO_4$). That is, blending with 4% PVDF-*g*-PSPMA and 1.5% $KClO_4$ in PVDF casting solution may result in interaction between $KClO_4$ and phase inversion kinetics, resulting in the formation of a crack-free PVDF MF membrane (A3). This implies that cracks can be prevented during membrane preparation despite blending with excessive hydrophilic graft copolymer (i.e., PVDF-*g*-PSPMA). Moreover, higher PSD peak and smoother membrane surface, as well as increased hydrophilicity (compared to the pristine PVDF membrane), are also successfully achieved by blending with $KClO_4$ and PVDF-*g*-PSPMA. The aforementioned properties ultimately allow the A3 membrane to show higher cumulative permeate volume, a slower rate of decline in flux decline (from 0 to 10 min), and greater flux recovery than those of the commercially available PVDF membrane during microfiltration of HA solution, even though it is relatively more hydrophobic than commercial membrane. Based on characterizations, it is suggested that blending with 4% PVDF-*g*-PSPMA and 1.5% $KClO_4$ may be a viable method for preventing crack formation and controlling average pore size (i.e., about 220 nm) of PVDF MF membrane. In addition, the comparisons of flux performances for A1, A2, A3, and commercial membranes also suggest that blending with PVDF-*g*-PSPMA and $KClO_4$ enhances antifouling characteristics of PVDF MF membrane significantly. Antifouling characteristics of the crack-free membrane (A3) would help to regenerate a fouled membrane and solve fouling problem such as flux decline during treatment of water containing HA. Further studies are needed to discuss the relationship between antifouling characteristics enhancement and improved surface zeta-potential, which may be attributable to blending with PVDF-*g*-PSPMA and $KClO_4$, as well as flux performance through several kinds of feed solutions.

DOI: 10.1021/acsami.5b03797
ACS Appl. Mater. Interfaces 2015, 7, 16466−16477

AUTHOR INFORMATION

Corresponding Author

*Tel.: +82 (2) 2123-2757. Fax: +82 (2) 312-6401. E-mail: minbr345@yonsei.ac.kr.

Notes

The authors declare no competing financial interest.

ACKNOWLEDGMENTS

This work was partly supported by a National Research Foundation (NRF) of Korea grant funded by the Korean government (MEST) (No. 2011-0029161). The authors would like to thank the NRF and the Korean government (MEST) for providing financial support.

REFERENCES

(1) Kazemimoghadam, M.; Mohammadi, T. Chemical Cleaning of Ultrafiltration Membranes in the Milk Industry. *Desalination* **2007**, *204* (1), 213−218.

(2) Figueroa, R. A. R.; Cassano, A.; Drioli, E. Ultrafiltration of Orange Press Liquor: Optimization for Permeate Flux and Fouling Index by Response Surface Methodology. *Sep. Purif. Technol.* **2011**, *80* (1), 1−10.

(3) Chabeaud, A.; Vandanjon, L.; Bourseau, P.; Jaouen, P.; Guérard, F. Fractionation by Ultrafiltration of a Saithe Protein Hydrolysate (Pollachius Virens): Effect of Material and Molecular Weight Cut-off on the Membrane Performances. *J. Food Eng.* **2009**, *91* (3), 408−414.

(4) Chen, D.; Hickner, M. A.; Agar, E.; Kumbur, E. C. Optimized Anion Exchange Membranes for Vanadium Redox Flow Batteries. *ACS Appl. Mater. Interfaces* **2013**, *5* (15), 7559−7566.

(5) Lai, A. N.; Wang, L. S.; Lin, C. X.; Zhuo, Y. Z.; Zhang, Q. G.; Zhu, A.; Liu, Q. L. Phenolphthalein−based Poly (Arylene Ether Sulfone Nitrile) s Multiblock Copolymers as Anion Exchange Membranes for Alkaline Fuel Cells. *ACS Appl. Mater. Interfaces* **2015**, *7* (15), 8284−8292.

(6) Bergamasco, R.; Da Silva, F. V.; Arakawa, F. S.; Yamaguchi, N. U.; Reis, M. H. M.; Tavares, C. J.; De Amorim, M. T. P. S.; Tavares, C. R. G. Drinking Water Treatment in a Gravimetric Flow System with TiO 2 Coated Membranes. *Chem. Eng. J.* **2011**, *174* (1), 102−109.

(7) Chen, F.; Peldszus, S.; Peiris, R. H.; Ruhl, A. S.; Mehrez, R.; Jekel, M.; Legge, R. L.; Huck, P. M. Pilot-scale Investigation of Drinking Water Ultrafiltration Membrane Fouling Rates Using Advanced Data Analysis Techniques. *Water Res.* **2014**, *48*, 508−518.

(8) Ong, Y. K.; Li, F. Y.; Sun, S.-P.; Zhao, B.-W.; Liang, C.-Z.; Chung, T.-S. Nanofiltration Hollow Fiber Membranes for Textile Waste Water Treatment: Lab-scale and Pilot-scale Studies. *Chem. Eng. Sci.* **2014**, *114*, 51−57.

(9) Phuntsho, S.; Lotfi, F.; Hong, S.; Shaffer, D. L.; Elimelech, M.; Shon, H. K. Membrane Scaling and Flux Decline during Fertiliser-drawn Forward Osmosis Desalination of Brackish Groundwater. *Water Res.* **2014**, *57*, 172−182.

(10) Zhang, S.; Wang, K. Y.; Chung, T.-S.; Jean, Y.; Chen, H. Molecular Design of the Cellulose Ester-based Forward Osmosis Membranes for Desalination. *Chem. Eng. Sci.* **2011**, *66* (9), 2008−2018.

(11) Wang, J.; Lang, W.-Z.; Xu, H.-P.; Zhang, X.; Guo, Y.-J. Improved Poly (Vinyl Butyral) Hollow Fiber Membranes by Embedding Multi-walled Carbon Nanotube for the Ultrafiltrations of Bovine Serum Albumin and Humic Acid. *Chem. Eng. J.* **2015**, *260*, 90−98.

(12) Alzahrani, S.; Mohammad, A.; Hilal, N.; Abdullah, P.; Jaafar, O. Comparative Study of NF and RO Membranes in the Treatment of Produced Water—Part I: Assessing Water Quality. *Desalination* **2013**, *315*, 18−26.

(13) Lubello, C.; Gori, R.; Nicese, F. P.; Ferrini, F. Municipal-treated Wastewater Reuse for Plant Nurseries Irrigation. *Water Res.* **2004**, *38* (12), 2939−2947.

(14) Fletcher, H.; Mackley, T.; Judd, S. The Cost of a Package Plant Membrane Bioreactor. *Water Res.* **2007**, *41* (12), 2627−2635.

(15) Hirani, Z. M.; Bukhari, Z.; Oppenheimer, J.; Jjemba, P.; LeChevallier, M. W.; Jacangelo, J. G. Characterization of Effluent Water Qualities from Satellite Membrane Bioreactor Facilities. *Water Res.* **2013**, *47* (14), 5065−5075.

(16) Liang, S.; Kang, Y.; Tiraferri, A.; Giannelis, E. P.; Huang, X.; Elimelech, M. Highly Hydrophilic Polyvinylidene Fluoride (PVDF) Ultrafiltration Membranes via Postfabrication Grafting of Surface-tailored Silica Nanoparticles. *ACS Appl. Mater. Interfaces* **2013**, *5* (14), 6694−6703.

(17) Sailaja, G. S.; Zhang, P.; Anilkumar, G. M.; Yamaguchi, T. Aniosotropically Organized LDH on PVDF: A Geometrically Templated Electrospun Substrate for Advanced Anion Conducting Membranes. *ACS Appl. Mater. Interfaces* **2015**, *7* (12), 6397−6401.

(18) Garain, S.; Sinha, T. K.; Adhikary, P.; Henkel, K.; Sen, S.; Ram, S.; Sinha, C.; Schmeißer, D.; Mandal, D. Self-Poled Transparent and Flexible UV-light Emitting Cerium Complex-PVDF Composite: A High Performance Nanogenerator. *ACS Appl. Mater. Interfaces* **2014**, *7* (2), 1298−1307.

(19) Gilron, J.; Hasson, D. Calcium Sulphate Fouling of Reverse Osmosis Membranes: Flux Decline Mechanism. *Chem. Eng. Sci.* **1987**, *42* (10), 2351−2360.

(20) Cho, J.; Amy, G.; Pellegrino, J. Membrane Filtration of Natural Organic Matter: Initial Comparison of Rejection and Flux Decline Characteristics with Ultrafiltration and Nanofiltration Membranes. *Water Res.* **1999**, *33* (11), 2517−2526.

(21) Huyskens, C.; Brauns, E.; Van Hoof, E.; Diels, L.; De Wever, H. Validation of a Supervisory Control System for Energy Savings in Membrane Bioreactors. *Water Res.* **2011**, *45* (3), 1443−1453.

(22) Yuan, W.; Zydney, A. L. Humic Acid Fouling during Microfiltration. *J. Membr. Sci.* **1999**, *157* (1), 1−12.

(23) Liu, B.; Chen, C.; Li, T.; Crittenden, J.; Chen, Y. High Performance Ultrafiltration Membrane Composed of PVDF Blended with Its Derivative Copolymer PVDF-g-PEGMA. *J. Membr. Sci.* **2013**, *445*, 66−75.

(24) Sui, Y.; Wang, Z.; Gao, X.; Gao, C. Antifouling PVDF Ultrafiltration Membranes Incorporating PVDF-g-PHEMA Additive via Atom Transfer Radical Graft Polymerizations. *J. Membr. Sci.* **2012**, *413*, 38−47.

(25) Abed, M. M.; Kumbharkar, S.; Groth, A.; Li, K. Economical Production of PVDF-g-POEM for Use as a Blend in Preparation of PVDF Based Hydrophilic Hollow Fibre Membranes. *Sep. Purif. Technol.* **2013**, *106*, 47−55.

(26) Möckel, D.; Staude, E.; Guiver, M. D. Static Protein Adsorption, Ultrafiltration Behavior and Cleanability of Hydrophilized Polysulfone Membranes. *J. Membr. Sci.* **1999**, *158* (1), 63−75.

(27) Woo, S. H.; Kim, K.-M.; Park, J.; Min, B. R. Preparation and Characterization of Poly (vinylidene fluoride) (PVDF) Membrane. *Chem. Lett.* **2015**, *44* (1), 85−87.

(28) Kim, Y. W.; Lee, D. K.; Lee, K. J.; Kim, J. H. Single-step Synthesis of Proton Conducting Poly (Vinylidene Fluoride)(PVDF) Graft Copolymer Electrolytes. *Eur. Polym. J.* **2008**, *44* (3), 932−939.

(29) Rahimpour, A.; Madaeni, S. S.; Mansourpanah, Y. Fabrication of Polyethersulfone (PES) Membranes with Nano-porous Surface Using Potassium Perchlorate ($KClO_4$) as an Additive in the Casting Solution. *Desalination* **2010**, *258* (1), 79−86.

(30) Jena, A.; Gupta, K. Characterization of Pore Structure of Filtration Media. *Fluid/Part. Sep. J.* **2002**, *14* (3), 227−241.

(31) Li, D.; Frey, M. W.; Joo, Y. L. Characterization of Nanofibrous Membranes with Capillary Flow Porometry. *J. Membr. Sci.* **2006**, *286* (1), 104−114.

(32) Shao, J.; Hou, J.; Song, H. Comparison of Humic Acid Rejection and Flux Decline during Filtration with Negatively Charged and Uncharged Ultrafiltration Membranes. *Water Res.* **2011**, *45* (2), 473−482.

(33) Liao, Y.; Wang, R.; Tian, M.; Qiu, C.; Fane, A. G. Fabrication of Polyvinylidene Fluoride (PVDF) Nanofiber Membranes by Electro-

DOI: 10.1021/acsami.5b03797
ACS Appl. Mater. Interfaces 2015, 7, 16466−16477

spinning for Direct Contact Membrane Distillation. *J. Membr. Sci.* **2013**, *425*, 30−39.
(34) Lee, N.; Amy, G.; Croué, J.-P.; Buisson, H. Morphological Analyses of Natural Organic Matter (NOM) Fouling of Low-pressure Membranes (MF/UF). *J. Membr. Sci.* **2005**, *261* (1), 7−16.
(35) Kim, J. Y.; Lee, H. K.; Kim, S. C. Surface Structure and Phase Separation Mechanism of Polysulfone Membranes by Atomic Force Microscopy. *J. Membr. Sci.* **1999**, *163* (2), 159−166.
(36) Lin, D.-J.; Chang, C.-L.; Huang, F.-M.; Cheng, L.-P. Effect of Salt Additive on the Formation of Microporous Poly (Vinylidene Fluoride) Membranes by Phase Inversion from $LiClO_4$/water/DMF/PVDF system. *Polymer* **2003**, *44* (2), 413−422.
(37) Yeow, M.; Liu, Y.; Li, K. Preparation of Porous PVDF Hollow Fibre Membrane via a Phase Inversion Method Using Lithium Perchlorate ($LiClO_4$) as an Additive. *J. Membr. Sci.* **2005**, *258* (1), 16−22.
(38) Košutić, K.; Kunst, B. RO and NF Membrane Fouling and Cleaning and Pore Size Distribution Variations. *Desalination* **2002**, *150* (2), 113−120.
(39) Fane, A.; Fell, C.; Waters, A. The Relationship Between Membrane Surface Pore Characteristics and Flux for Ultrafiltration Membranes. *J. Membr. Sci.* **1981**, *9* (3), 245−262.

DOI: 10.1021/acsami.5b03797
ACS Appl. Mater. Interfaces 2015, 7, 16466−16477